Structure–Property Relationships

Deutsche Ausgabe: DOI: 10.1002/ange.201411772
Internationale Ausgabe: DOI: 10.1002/anie.201411772

Tailored Synthesis of a Nonlinear Optical Phosphate with a Short Absorption Edge**

Sangen Zhao, Pifu Gong, Siyang Luo, Lei Bai, Zheshuai Lin, Yuanyuan Tang, Yuelan Zhou, Maochun Hong, and Junhua Luo**

Abstract: *A nonlinear optical phosphate $Ba_5P_6O_{20}$ was rationally developed by a tailored synthetic approach based on the use of flexible $[P_3O_{10}]^{5-}$ units. The phosphate exhibits a very short absorption edge of $\lambda = 167$ nm, which is among the shortest known in phase-matchable phosphates. First-principles electronic structure analysis elucidated the origin of the changes in the optical properties, and specifically in the absorption edge, of the material. Such a tailored synthetic approach provides a new opportunity to design nonlinear optical materials with short absorption edges.*

Nonlinear optical (NLO) materials can efficiently expand the fixed (or limited) wavelengths available from laser sources and as a result play a significant role in laser science and technology, particularly for applications in the ultraviolet (UV) and deep-UV regions, such as ultrafine spectral analysis, precise micromanufacturing, and photochemistry.[1] To be optically applicable, a NLO material must satisfy several fundamental requirements: it should have a large SHG response (SHG = second harmonic generation), a wide optical transparency window, and phase-matching capability.[1a] Over the past several decades, great efforts have been made on the design and synthesis of NLO materials with enhanced SHG performances, leading to the discovery of many highly NLO-active materials. These materials include π-orbital systems[2] such as $CsPbCO_3F$,[2a] $Cd_4BiO(BO_3)_3$,[2b] and $Pb_2B_5O_9I$,[2c] second-order Jahn–Teller cations in oxide materials[3] such as $BaTeMo_2O_9$,[3a] NaI_3O_8,[3b] and $ATi(IO_3)_6$ (A = Li, Na, K, Rb, Cs, Tl),[3c,d] as well as chalcogenide-metalates[4] such as $LiAsS_2$[4a] and $BaGa_4Se_7$.[4b] However, most of these materials are not suitable for the generation of deep-UV coherent light as it requires a very wide optical transparency window down to $\lambda = 200$ nm. To date, $KBe_2BO_3F_2$ (KBBF)[5] is the only NLO crystal which can be practically applied in the deep-UV region, but it contains the toxic element beryllium and it is particularly difficult to grow crystals of the material. The other newly developed deep-UV NLO materials[6] are still at the laboratory stage. On the other hand, despite the commonly accepted view that the introduction of some main group ions (e.g. halide F^- ions, alkaline cations, and alkaline-earth cations) is favorable to form an optical transparency window at short wavelengths,[7] there are still a lack of studies that show how to rationally construct NLO materials with an extended transparency window at short wavelengths.[8] Moreover, it is very difficult to shorten the absorption edges of deep-UV NLO materials as they almost approach the theoretical limits of NLO materials.[9] Therefore, as new deep-UV NLO materials are in urgent demand, the molecular design, especially in terms of the optical transparency window, is crucial for the development of these important optoelectronic functional materials.

To date, deep-UV NLO materials are almost exclusively limited to borates, except for several newly discovered phosphates.[10] In particular, Chen and co-workers reported the first non-boron-containing deep-UV NLO phosphates, $Ba_3P_3O_{10}X$ (X = Cl, Br), which consist of $[P_3O_{10}]^{5-}$ short chains and are transparent down to $\lambda = 180$ nm and $\lambda < 200$ nm, respectively.[10a] According to structural analysis, the authors found the $[P_3O_{10}]^{5-}$ units feature a structural flexibility that leads to the crystallographic asymmetry. In this work, we attempt to develop deep-UV NLO phosphates with extended transparency windows by a tailored synthetic approach, namely, removing the X^- ions and charge-compensating Ba^{2+} cations from $Ba_3P_3O_{10}X$ while utilizing the flexible $[P_3O_{10}]^{5-}$ ions to maintain the structural asymmetry of the crystal:

$$2\,Ba_3P_3O_{10}X - Ba^{2+}X^-_2 \rightarrow Ba_5P_6O_{20} \quad (1)$$

The resultant $Ba_5P_6O_{20}$ consists of flexible $[P_3O_{10}]^{5-}$ units and is structurally analogous to $Ba_3P_3O_{10}X$, but exhibits a markedly shortened absorption edge of $\lambda = 167$ nm, which is among the shortest known in phase-matchable phosphates. First-principles calculations are carried out to elucidate the origin of optical properties.

Polycrystalline samples of $Ba_5P_6O_{20}$ were synthesized by high-temperature solid-state reaction techniques. The experimental powder X-ray diffraction (XRD) patterns are in good

[*] Dr. S. Zhao, Y. Tang, Y. Zhou, Prof. M. Hong, Prof. J. Luo
Key Laboratory of Optoelectronic Materials Chemistry and Physics
Fujian Institute of Research on the Structure of Matter
Chinese Academy of Sciences, Fuzhou, Fujian, 350002 (P.R. China)
E-mail: jhluo@fjirsm.ac.cn
P. Gong, Dr. S. Luo, Dr. L. Bai, Prof. Z. Lin
Beijing Center for Crystal R&D, Key Lab of Functional Crystals and Laser Technology of Chinese Academy of Sciences
Technical Institute of Physics and Chemistry
Chinese Academy of Sciences, Beijing 100190 (China)
E-mail: zslin@mail.ipc.ac.cn

[**] This work was financially supported by NSFC of China (21222102, 21373220, 51402296, 21171166, 11174297, and 11474292), the National Basic Research Project of China (2011CB922204 and 2011CB935904), and the opening fund of Key Laboratory of Functional Crystals and Laser Technology, TIPC, CAS (FCLT 201306). S.Z. is grateful for support from the Chunmiao Project of Haixi Institute of Chinese Academy of Sciences (CMZX-2015-003).
Supporting information for this article is available on the WWW under http://dx.doi.org/10.1002/anie.201411772.

agreement with the calculated patterns based on single-crystal XRD analysis (see Figure S2 in the Supporting Information). Single crystals of $Ba_5P_6O_{20}$ (Figure S3) were grown through spontaneous crystallization with a Cs_2O–P_2O_5 flux. The crystal structure of $Ba_5P_6O_{20}$ was determined by single-crystal XRD using graphite-monochromatized Mo Kα radiation ($\lambda =$ 0.71073 Å) at 100(2) K (for detailed crystallographic data, see Tables S1–S3). The inductively coupled plasma element analysis gave a molar ratio of Ba:P = 5:6.3.

$Ba_5P_6O_{20}$ crystallizes in the non-centrosymmetric polar orthorhombic space group of $Pca2_1$.[11] As shown in Figure 1 a, the crystal structure of $Ba_5P_6O_{20}$ consists of four repeating sheets in a packing manner of $ABCB'ABCB'$. The B and B' sheets are related to each other through an a glide plane. There are twelve crystallographically independent phosphorus atoms which are four-coordinated with oxygen atoms to form PO_4 tetrahedra. These tetrahedra further share corners to construct four sets of discrete $[P_3O_{10}]^{5-}$ trimers: one in A sheets, two in B and B' sheets, and the final trimer in C sheets (see Figure 1 b–d). PO_4 tetrahedra are distorted with O-P-O angles in the range of 97.1(4)–118.0(4)° and P–O bonds in the range of 1.486(7)–1.681(7) Å. Such distortions result in non-centrosymmetric local coordination without any mirror plane symmetry in the $[P_3O_{10}]^{5-}$ trimers, just as in the cases of $Ba_3P_3O_{10}X$ (X = Cl, Br).[10a] Additionally, Ba atoms are 7-, 8-, or 9-coordinated to form locally non-centrosymmetric BaO_7/BaO_8/BaO_9 polyhedra with Ba–O bond lengths ranging from 2.578(7) Å to 3.003(7) Å.

$Ba_5P_6O_{20}$ is structurally analogous to $Ba_3P_3O_{10}X$.[10a] However, although it crystallizes in the same space group as $Ba_3P_3O_{10}Cl$ ($Pca2_1$), it is somewhat different from that of $Ba_3P_3O_{10}Br$ ($P2_12_12_1$). This difference may originate from the different size effect of halide X^- ions.[10a] As shown in Figure S4, the configurations and spatial packing of $[P_3O_{10}]^{5-}$ ions in $Ba_3P_3O_{10}X$ are similar to those in the A and C sheets of $Ba_5P_6O_{20}$. $Ba_3P_3O_{10}Cl$ consists of one repeating sheet A in an AAA stacking sequence, while $Ba_3P_3O_{10}Br$ contains two repeating sheets A and A' in an $A'AA'A$ stacking sequence. As a result, the cell parameter b (19.1788(3) Å) of $Ba_5P_6O_{20}$ is about four times that of $Ba_3P_3O_{10}Cl$ ($b = 5.5968(4)$ Å) and is about twice that of $Ba_3P_3O_{10}Br$ ($b = 11.364(3)$ Å). As indicated in Figure 1, in the A and C sheets the P-P-P angles of $[P_3O_{10}]^{5-}$ trimers are 112.8(1)° and 112.5(1)°, respectively, which are slightly larger than those in $Ba_3P_3O_{10}Cl$ (109.0(1)°; see Figure S4b) and $Ba_3P_3O_{10}Br$ (108.0(1)°, see Figure S4d). In the B and B' sheets, the $[P_3O_{10}]^{5-}$ trimers exhibit quite different configurations with nearly orthogonal P-P-P angles of 91.9(1)° and 92.9(1)°. Evidently, the $[P_3O_{10}]^{5-}$ trimers in $Ba_5P_6O_{20}$ are structurally flexible. When the $Ba^{2+}X^-_2$ is removed from the structure of $Ba_3P_3O_{10}X$, the flexible $[P_3O_{10}]^{5-}$ ions adjust their bending and folding geometry and further modify the stacking pattern to maintain the crystallographic asymmetry. In this way, the tailored synthesis of non-centrosymmetric compounds has been realized by utilizing flexible building units.

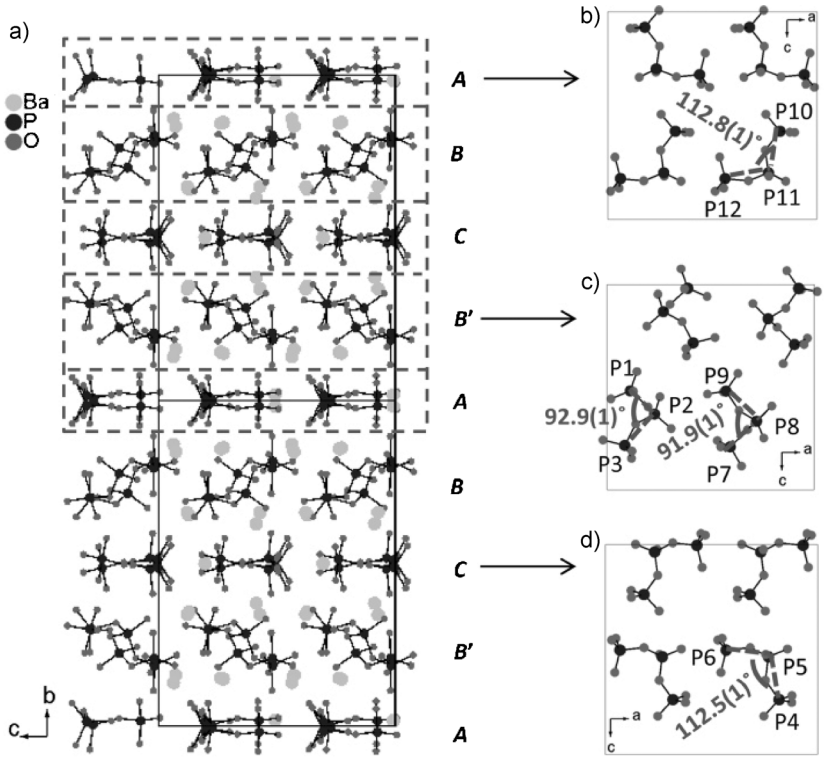

Figure 1. a) Crystal structure of $Ba_5P_6O_{20}$. Spatial packing of $[P_3O_{10}]^{5-}$ trimers in b) A sheets, c) B' sheets, and d) C sheets. The B and B' sheets are related to each other through an a glide plane. The size of the P-P-P angles is indicated. Ba atoms are omitted for clarity in (b–d).

As $Ba_5P_6O_{20}$ is non-centrosymmetric, it is expected to be NLO active. We carried out powder second-harmonic generation (SHG) tests by the Kurtz–Perry method[12] with a Q-switched Nd:YAG laser of $\lambda = 1064$ nm. Polycrystalline KH_2PO_4 (KDP) samples were used as the reference materials. As shown in Figure 2 a, the SHG intensities increase with increasing particle sizes before they reach a maximum SHG intensity that does not increase with particle size. According to the rule proposed by Kurtz and Perry,[12] $Ba_5P_6O_{20}$ is phase matchable. With a particle size of 250–300 μm, its SHG efficiency is about 0.8 times that of KDP. This value is comparable to the other deep-UV NLO phosphates, including the structurally analogous $Ba_3P_3O_{10}Cl$ (0.6 KDP) and $Ba_3P_3O_{10}Br$ (0.5 KDP),[10a] $RbBa_2(PO_3)_5$ (1.4 KDP), $Rb_2Ba_3(P_2O_7)_2$ (0.3 KDP),[10b] and $CsLa(PO_3)_4$ (0.5 KDP).[10c] The deep-UV transmittance spectrum of a $Ba_5P_6O_{20}$ single crystal was collected in the spectral range of $\lambda = 120$–220 nm on a McPherson VUVas2000 spectrophotometer. As shown in Figure 2 b, $Ba_5P_6O_{20}$ has a short absorption edge of $\lambda = 167$ nm (corresponding to a very large bandgap of 7.43 eV) which is markedly shorter than those of the structurally analogous $Ba_3P_3O_{10}Cl$ (180 nm) and $Ba_3P_3O_{10}Br$ (< 200 nm).[10a] To our knowl-

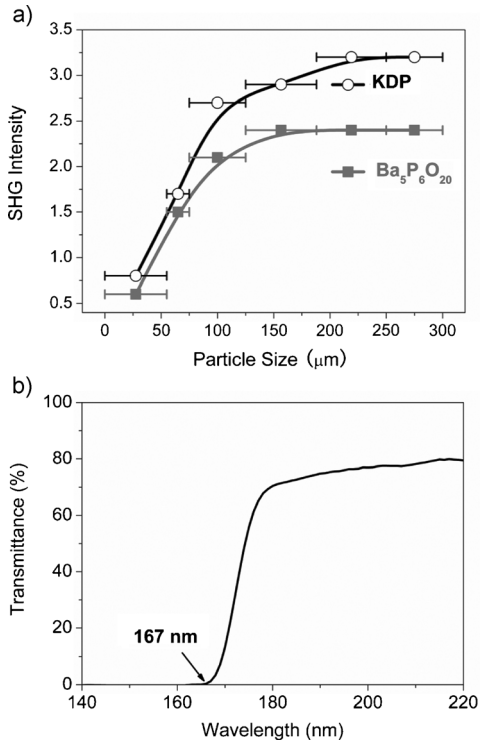

Figure 2. a) SHG intensity versus particle size curves at $\lambda = 1064$ nm. b) Deep-UV transmittance spectrum of $Ba_5P_6O_{20}$. KDP samples serve as the references. In (a) the solid curves are a guide for the eye and not a fit to the data.

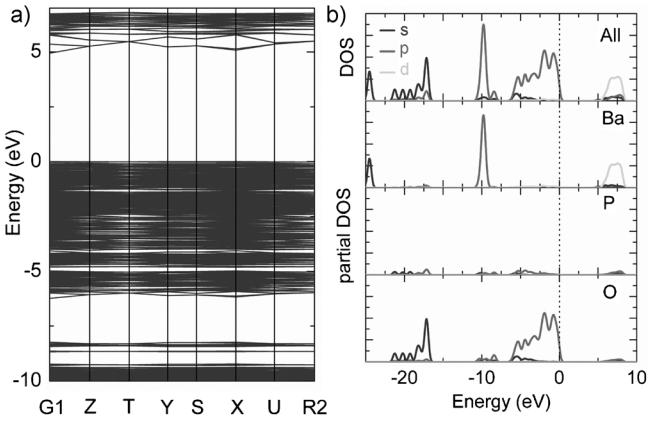

Figure 3. a) Electronic band structure of $Ba_5P_6O_{20}$. b) DOS and partial DOS projected on the constitutional atoms of $Ba_5P_6O_{20}$.

edge, the absorption edge of $Ba_5P_6O_{20}$ is among the shortest known in phase-matchable phosphates.[13] From the point of view of practical applications, such a blue shift of the absorption edge is very useful. For instance, it means that the material $Ba_5P_6O_{20}$ could generate coherent light at $\lambda =$ 177.3 nm, a laser which is crucial to a range of advanced scientific instruments.[7a]

To elucidate the origin of the optical properties of $Ba_5P_6O_{20}$, we performed first-principles calculations by the plane-wave pseudopotential method implemented in the CASTEP package.[14] Figure 3 a and 3 b display the electronic band structure and the density of states (DOS) and partial DOS projected on the constitutional atoms, respectively. As shown in Figure 3 a, $Ba_5P_6O_{20}$ is a direct-gap crystal. As a result of the notorious problem of exchange-correlation functionals,[15] the predicted energy bandgap (4.94 eV) is smaller than the experimental value (7.43 eV). However, our previous studies demonstrated that the calculated electronic band dispersions are well reproduced for the UV NLO crystals,[16] so the analysis on the calculated electronic structure can obtain an understanding of the origin of the optical properties for $Ba_5P_6O_{20}$. Several electronic characteristics can be deduced from Figure 3 b. a) The region lower than −8 eV is composed of the isolated inner-shell states with barium 4s4p, phosphorus 2s2p, and oxygen 2s orbitals, which have little interaction with neighboring atoms. b) The upper part of the valence band is mainly composed of the p orbitals of oxygen (2p) and phosphorus (3p), indicating that there are relatively strong covalent bonds between O and P atoms. c) The bottom of the conduction band consists of a mixture of the orbitals on all of the constituent atoms. As the optical response of a crystal mainly originates from the electronic transitions between valence-band and conduction-band states close to the bandgap,[17] it is P-O groups (namely, the $[P_3O_{10}]^{5-}$ groups) that mainly determine the magnitude of the energy bandgap for $Ba_5P_6O_{20}$.

As $Ba_5P_6O_{20}$ and $Ba_3P_3O_{10}X$ show analogous structures, we considered that the halide X^- ions may be responsible to the difference in the UV transparency windows between the compounds. The DOS and partial DOS of $Ba_3P_3O_{10}X$ (see Figure 4 a, b in Ref. [10a]) clearly reveal that Cl 3p orbitals or Br 4p orbitals are very localized with the full width at half maximum (FWHM) values less than 1 eV; they have little hybridization with other orbitals and push the electronic level at the valence band maximum upwards, thus narrowing the energy bandgap. This result confirmed our view that the absence of halide Cl^-/Br^- ions is responsible for the extended transparency window of $Ba_5P_6O_{20}$. Interestingly, this result is in contrast to the case of KBBF[18] in which energy spanning of the 2p orbitals for F^- ions is more than 4 eV; the rather large hybridization (between the orbitals on fluorine and those on the neighboring ions) decreases the energy of the valence band and causes the blue shift of the absorption edge. Indeed, it is a challenge to design NLO materials with shortened absorption edges, especially in the deep-UV spectral region, as it involves subtle changes in the relationships between composition, structure, and properties.[9]

In summary, we have synthesized a new deep-UV NLO material $Ba_5P_6O_{20}$ based on flexible $[P_3O_{10}]^{5-}$ building units. $Ba_5P_6O_{20}$ inherits the structural features of the first deep-UV NLO phosphates $Ba_3P_3O_{10}X$, but exhibits a markedly shortened absorption edge of $\lambda = 167$ nm, which is among the shortest in phase-matchable phosphates. Such a blue shift of the absorption edge makes the application of $Ba_5P_6O_{20}$ possible for some significant deep-UV NLO applications. First-principles calculations confirmed that the shortened absorption edge is ascribed to the absence of halide Cl^-/Br^- ions in comparison with $Ba_3P_3O_{10}X$. Interestingly, this result is somewhat in contrast to the commonly accepted view that the

presence of F^- ions can cause a blue shift in the absorption edge. We believe these findings will shed useful insights into the development of new deep-UV NLO materials. Moreover, the tailored synthetic approach based on flexible building units provides an opportunity to design new structure-directing functional materials.

Experimental Section

Polycrystalline samples of $Ba_5P_6O_{20}$ were synthesized by high-temperature solid-state reaction techniques. A mixture of $BaCO_3$ (99%) and $(NH_4)_2HPO_4$ (99%) in stoichiometric proportions was thoroughly ground, heated to 823 K at a rate of 50 K h^{-1}, and then sintered at this temperature for 24 h. The products were ground thoroughly, heated to 1050 K at a rate of 50 K h^{-1}, and then sintered at this temperature for 120 h with several intermediate grindings. Powders of $Ba_5P_6O_{20}$ were obtained. The phase purity was confirmed by powder XRD, which was carried out at room temperature on a Rigaku MiniFlex II diffractometer equipped with Cu Kα radiation.

Single crystals of $Ba_5P_6O_{20}$ were grown through spontaneous crystallization with a Cs_2O–P_2O_5 flux. Powdered $Ba_5P_6O_{20}$, analytically pure Cs_2CO_3, and $(NH_4)_2HPO_4$ were mixed at a molar ratio of 2:3:8 in a platinum crucible, melted at 1273 K in a temperature-programmable electric furnace, and then held at this temperature for 24 h to ensure that the melt was homogenized. The melt was allowed to cool at a rate of 1 K h^{-1} until plate-like $Ba_5P_6O_{20}$ crystals crystallized at the surface of the melt. The temperature was subsequently decreased to room temperature at a rate of 25 K h^{-1}. Finally, colorless, transparent $Ba_5P_6O_{20}$ crystals (Figure S3) were physically separated from the matrix.

A colorless $Ba_5P_6O_{20}$ crystal ($0.15 \times 0.07 \times 0.05$ mm^3) was selected using an optical microscope for single-crystal XRD analysis. The diffraction data were collected by using graphite-monochromatized Mo Kα radiation ($\lambda = 0.71073$ Å) at 100(2) K on an Agilent SuperNova Dual diffractometer with an Atlas detector. The collection of the intensity data, cell refinement, and data reduction were carried out with the program CrysAlisPro.[19] The structure was solved by the direct method with program SHELXS and refined with the least-squares program SHELXL.[20] Final refinements include anisotropic displacement parameters. The structure was verified using the ADDSYM algorithm from the program PLATON,[21] and no higher symmetry was found.

Elemental analysis was performed by using a Jobin Yvon Ultima2 inductively coupled plasma optical emission spectrometer (ICP-OES) with Sepex Certiprep standards. The crystal samples were dissolved in aqua regia at the boiling point for 1 h.

Powder SHG measurements were performed with a Q-switched Nd:YAG laser at a wavelength of $\lambda = 1064$ nm. Polycrystalline samples were ground and sieved into the following particle size ranges: 0–55 μm, 55–75 μm, 75–125 μm, 125–188 μm, 188–250 μm, and 250–300 μm. The samples were pressed between glass slides and secured with tape in 1 mm-thick aluminum holders containing an 8 mm diameter hole. They were then placed into a light-tight box and irradiated with the laser of $\lambda = 1064$ nm. The intensity of the frequency-doubled output emitted from the samples was collected by a photomultiplier tube. Crystalline KDP was also ground and sieved into the same particle size ranges and used as the reference.

The first-principles electronic structure calculations were performed using the CASTEP code[14] based on density functional theory.[22] The norm-conserving pseudopotentials[23] and local density approximation[24] with CA-PZ functionals were chosen to describe the exchange and correlation potentials. The cutoff energy for the plane wave basis was set to be 900 eV. The *k*-point sampling in the Brillioun zone was set to be $2 \times 2 \times 1$, according to the Monkhorst–Pack scheme.[25]

Keywords: density functional calculations · nonlinear optics · solid-state structures · structure–property relationships · X-ray diffraction

How to cite: *Angew. Chem. Int. Ed.* **2015**, *54*, 4217–4221
Angew. Chem. **2015**, *127*, 4291–4295

[1] a) P. Becker, *Adv. Mater.* **1998**, *10*, 979–992; b) T. Sasaki, Y. Mori, M. Yoshimura, Y. K. Yap, T. Kamimura, *Mater. Sci. Eng. R* **2000**, *30*, 1–54; c) C. T. Chen, T. Sasaki, R. K. Li, Y. C. Wu, Z. S. Lin, Y. Mori, Z. G. Hu, J. Y. Wang, S. Uda, M. Yoshimura, Y. Kaneda, *Nonlinear Optical Borate Crystals: Principles and Applications*, Wiley-VCH, Weinheim, **2012**.

[2] a) G. H. Zou, L. Huang, N. Ye, C. S. Lin, W. D. Cheng, H. Huang, *J. Am. Chem. Soc.* **2013**, *135*, 18560–18566; b) W. L. Zhang, W. D. Cheng, H. Zhang, L. Geng, C. S. Lin, Z. Z. He, *J. Am. Chem. Soc.* **2010**, *132*, 1508–1509; c) Y. Z. Huang, L. M. Wu, X. T. Wu, L. H. Li, L. Chen, Y. F. Zhang, *J. Am. Chem. Soc.* **2010**, *132*, 12788–12789.

[3] a) H. S. Ra, K. M. Ok, P. S. Halasyamani, *J. Am. Chem. Soc.* **2003**, *125*, 7764–7765; b) D. Phanon, I. Gautier-Luneau, *Angew. Chem. Int. Ed.* **2007**, *46*, 8488–8491; *Angew. Chem.* **2007**, *119*, 8640–8643; c) H. Y. Chang, S. H. Kim, P. S. Halasyamani, K. M. Ok, *J. Am. Chem. Soc.* **2009**, *131*, 2426–2427; d) H. Y. Chang, S. H. Kim, K. M. Ok, P. S. Halasyamani, *J. Am. Chem. Soc.* **2009**, *131*, 6865–6873.

[4] a) T. K. Bera, J. H. Song, A. J. Freeman, J. I. Jang, J. B. Ketterson, M. G. Kanatzidis, *Angew. Chem. Int. Ed.* **2008**, *47*, 7828–7832; *Angew. Chem.* **2008**, *120*, 7946–7950; b) J. Y. Yao, D. J. Mei, L. Bai, Z. S. Lin, W. L. Yin, P. Z. Fu, Y. C. Wu, *Inorg. Chem.* **2010**, *49*, 9212–9216.

[5] Y. N. Xia, C. T. Chen, D. Y. Tang, B. C. Wu, *Adv. Mater.* **1995**, *7*, 79–81.

[6] a) S. G. Zhao, P. F. Gong, L. Bai, X. Xu, S. Q. Zhang, Z. H. Sun, Z. S. Lin, M. C. Hong, C. T. Chen, J. H. Luo, *Nat. Commun.* **2014**, *5*, 4019; b) S. C. Wang, N. Ye, *J. Am. Chem. Soc.* **2011**, *133*, 11458–11461; c) H. W. Huang, J. Y. Yao, Z. S. Lin, X. Y. Wang, R. He, W. J. Yao, N. X. Zhai, C. T. Chen, *Angew. Chem. Int. Ed.* **2011**, *50*, 9141–9144; *Angew. Chem.* **2011**, *123*, 9307–9310; d) H. P. Wu, H. W. Yu, S. L. Pan, Z. J. Huang, Z. H. Yang, X. Su, K. R. Poeppelmeier, *Angew. Chem. Int. Ed.* **2013**, *52*, 3406–3410; *Angew. Chem.* **2013**, *125*, 3490–3494.

[7] a) C. T. Chen, G. L. Wang, X. Y. Wang, Z. Y. Xu, *Appl. Phys. B* **2009**, *97*, 9–25; b) C. D. McMillen, J. T. Stritzinger, J. W. Kolis, *Inorg. Chem.* **2012**, *51*, 3953–3955.

[8] G. Zhang, Y. J. Li, K. Jiang, H. Y. Zeng, T. Liu, X. G. Chen, J. G. Qin, Z. S. Lin, P. Z. Fu, Y. C. Wu, C. T. Chen, *J. Am. Chem. Soc.* **2012**, *134*, 14818–14822.

[9] W. J. Yao, R. He, X. Y. Wang, Z. S. Lin, C. T. Chen, *Adv. Opt. Mater.* **2014**, *2*, 411–417.

[10] a) P. Yu, L. M. Wu, L. J. Zhou, L. Chen, *J. Am. Chem. Soc.* **2014**, *136*, 480–487; b) S. G. Zhao, P. F. Gong, S. Y. Luo, L. Bai, Z. S. Lin, C. M. Ji, T. L. Chen, M. C. Hong, J. H. Luo, *J. Am. Chem. Soc.* **2014**, *136*, 8560–8563; c) T. Q. Sun, P. Shan, H. Chen, X. W. Liu, H. D. Liu, S. L. Chen, Y. A. Cao, Y. F. Kong, J. J. Xu, *CrystEngComm* **2014**, *16*, 10497–10504.

[11] Crystal data for $Ba_5P_6O_{20}$: MW = 1192.52, colorless, $0.15 \times 0.07 \times 0.05$ mm^3, orthorhombic, space group: $Pca2_1$ (29), $a = 14.0871(2)$, $b = 19.1788(3)$, $c = 13.9437(2)$ Å, $V = 3767.22(10)$ Å^3, $Z = 8$, $F(000) = 4240$, $\mu = 10.907$ mm^{-1}, $T = 100(2)$ K; $R(\text{int}) = 0.0275$; the final refinement was converged with $R_1 = 0.0289$ and $wR_2 = 0.0693$; GOOF = 1.037; Flack parameter 0.196(19). CCDC-1026318 contains the supplementary crystallographic data for this paper. These data can be obtained free of charge from The Cambridge Crystallographic Data Centre via www.ccdc.cam.ac.uk/data_request/cif.

[12] S. K. Perry, T. T. Kurtz, *J. Appl. Phys.* **1968**, *39*, 3798–3813.

[13] V. G. Dimitriev, *Handbook of Nonlinear Optical Crystals*, Springer, Berlin, **1991**.
[14] a) M. C. Payne, M. P. Teter, D. C. Allan, T. A. Arias, J. D. Joannopoulos, *Rev. Mod. Phys.* **1992**, *64*, 1045 – 1097; b) S. J. Clark, M. D. Segall, C. J. Pickard, P. J. Hasnip, M. J. Probert, K. Refson, M. C. Payne, *Z. Kristallogr.* **2005**, *220*, 567 – 570.
[15] Z. S. Lin, X. X. Jiang, L. Kang, P. F. Gong, S. Y. Luo, M. H. Lee, *J. Phys. D* **2014**, *47*, 253001.
[16] R. He, H. W. Huang, L. Kang, W. J. Yao, X. X. Jiang, Z. S. Lin, J. G. Qin, C. T. Chen, *Appl. Phys. Lett.* **2013**, *102*, 231904.
[17] M. H. Lee, C. H. Yang, J. H. Jan, *Phys. Rev. B* **2004**, *70*, 335503.
[18] L. Kang, S. Y. Luo, H. W. Huang, T. Zheng, Z. S. Lin, C. T. Chen, *J. Phys. Condens. Matter* **2012**, *24*, 335503.
[19] *CrysAlisPro*, Version 1.171.36.28, Agilent Technologies, Santa Clara, CA, **2013**.
[20] G. M. Sheldrick, *Acta Crystallogr. Sect. A* **2008**, *64*, 112 – 122.
[21] A. L. Spek, *J. Appl. Crystallogr.* **2003**, *36*, 7 – 13.
[22] W. Kohn, *Rev. Mod. Phys.* **1999**, *71*, 1253 – 1266.
[23] J. S. Lin, A. Qteish, M. C. Payne, V. Heine, *Phys. Rev. B* **1993**, *47*, 4174 – 4180.
[24] W. Kohn, L. J. Sham, *Phys. Rev.* **1965**, *140*, A1133 – A1138.
[25] H. J. Monkhorst, J. D. Pack, *Phys. Rev. B* **1976**, *13*, 5188 – 5192.

Received: December 7, 2014
Revised: January 20, 2015
Published online: February 9, 2015

